Combustion and Flame 219, 13-19 (2020)
Preprint

On the Effect of Pressure on Soot Nanostructure: A Raman Spectroscopy Investigation

M. Commodo [*, 1], A.E. Karataş [2], G. De Falco [3], P. Minutolo [1], A. D'Anna [3], Ö.L. Gülder [*, 4]

[1] Istituto di Ricerche sulla Combustione, CNR, P.le Tecchio 80, 80125, Napoli, Italy

[2] Department of Aerospace Engineering, Ryerson University, 350 Victoria St., Toronto, Ontario M5B 2K3, Canada

[3] Università degli Studi di Napoli Federico II, Dipartimento di Ingegneria Chimica, dei Materiali e della Produzione Industriale - P.le Tecchio 80, 80125, Napoli, Italy

[4] University of Toronto Institute for Aerospace Studies, 4925 Dufferin Street, Toronto, Ontario M3H 5T6, Canada

* Corresponding Authors: Mario Commodo (commodo@cnr.it)
Ömer L. Gülder (ogulder@utias.utoronto.ca)

Combustion and Flame 219, 13-19 (2020)
Preprint

Abstract

Although the majority of existing combustion devices operate at high pressure conditions, most of our understanding of the soot formation process and soot physicochemical properties rely on studies performed at atmospheric pressure. Pressure is known to have nonlinear effects on combustion processes and a significant influence on soot formation; soot loading increases with increasing combustion pressure. Soot characteristics directly affect soot oxidation and optical/radiative properties, and it is desirable to have a better insight into them under high-pressure conditions. Indeed, due to scarcity of information on soot primary particles, aggregate morphology and soot nanostructure relevant to high-pressure combustion, there are challenges in handling the soot oxidation and radiation, particularly at engine-relevant conditions.

In this study, we perform Raman spectroscopy measurements on soot sampled from a set of laminar diffusion flames of ethylene at various pressures, ranging from atmospheric pressure to 12 bar. Our results show an increase in soot maturity as the pressure increases within the range of investigated pressures. In the examined co-flow flame pressure seem to have a indirect influence on soot nanostructure through an earlier inception of soot resulting in longer residence times of the carbon soot particles in the hot and reactive flame environment. In the examined flames, soot maturity, tracked through the size of graphitic domains, L_a, increases linearly with residence times. The longer residence time of soot in flame with increasing pressure could be the main cause of the higher degree of graphitization observed, which presumably reflect into a greater resistance to oxidation.

Combustion and Flame 219, 13-19 (2020)
Preprint

Introduction

Soot nanoparticles are known to have detrimental effects on human health, climate and air quality [1-3]. As a consequence of these concerns, significant research efforts have been put into understanding and explaining the chemical and physical processes behind the mechanisms of soot formation in fuel-rich flames. Although the majority of existing combustion technologies operate at pressure conditions ranging from moderate to high, most of our understanding of the soot formation process relies on studies performed at atmospheric condition. Pressure is known to strongly affect flame burning properties and soot formation [4]. It is established that pressure significantly increases soot loading [4]; as the pressure is increased in combustion chamber, more soot is formed and released to the exhaust, however the amount in the exhaust also depends on the extent of oxidation in the chamber. Nevertheless, soot concentration is not the only parameter to be considered. Particles size, morphology and nanostructure are also important since they directly affect oxidation rate as well as particle optical properties [5, 6]. However, probing and characterizing soot from high pressure environments is not a trivial task, and only a few attempts have been made so far [7-14]. Therefore, a clear understanding of the effect of pressure on particle size/morphology and nanostructure is far from being established firmly.

Recently, in an attempt to probe the dependence of soot nanostructure on pressure, we used Raman spectroscopy to characterize soot particles collected from several methane laminar diffusion flames operated under a variety of pressure conditions [10]. It was demonstrated that soot nanostructure was primarily affected by residence time rather than pressure [10]. Soot particles were shown to strongly graphitize when collected at increasing distances from the burner rim, while no differences were observable by changing the pressure of the system [10].

Compared to methane, ethylene flames are known to display significant differences in terms of soot formation and properties. In addition to the considerably different soot propensities, the dissimilar chemical features of the two fuels may also affect their soot characteristics, such as particle size, morphology and structure [9,11,15-17]. Thus, to complement our previous work [10] and

achieve a better understanding of the effect of pressure on soot nanostructures, we carried out Raman spectroscopy measurements in this work on soot samples extracted from ethylene diffusion flames at various pressures.

Experimental

Soot samples were collected thermophoretically from a set of nitrogen diluted ethylene laminar diffusion flames operated under various pressures. A high pressure combustion chamber capable of stabilizing laminar diffusion flames on a coflow burner was used. The high-pressure combustion chamber, housing the burner and the integrated thermophoretic soot sampling system has been thoroughly described elsewhere [8-12]. Briefly, the burner, installed in the high-pressure chamber, has an exit diameter of 3 mm. The thermophoretic sampling system consists of a circular sampling disk, a motor drive, and a programmable control system. To keep measurements at different pressures tractable, fuel mass flow rates were kept constant at all the pressures considered. The ethylene flow rate was 0.96 mg/s and fuel/nitrogen dilution was fixed at 1:2 by mass. Pressure was changed between 1 bar to 12 bar, and soot particles were collected at 2 and 10 mm above the burner rim, thus roughly in low and mid-height of the flames as depicted in Fig.1.

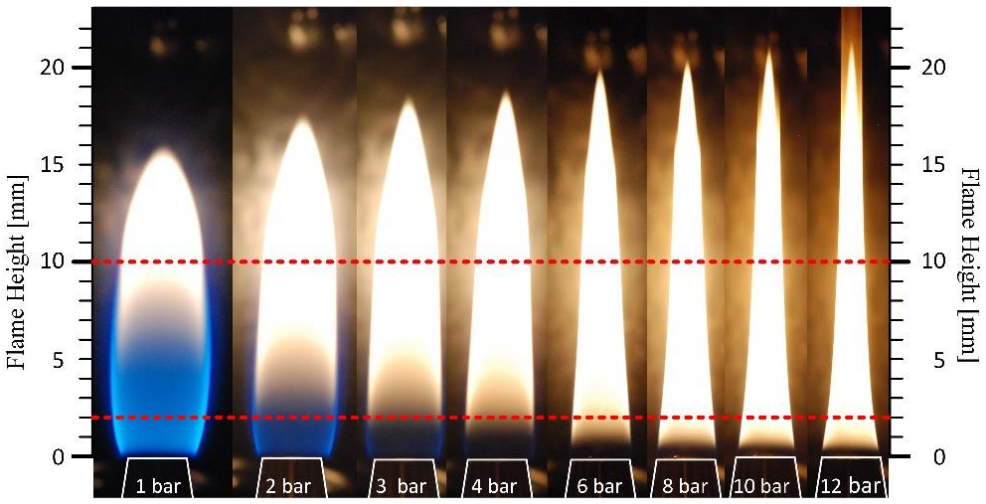

Figure 1. Photographs of the coflow laminar ethylene diffusion flames at different pressures. Red-dashed lines correspond to the sampling positions of 2 mm and 10 mm above the burner exit.

Samples for Raman spectroscopy measurements were collected by multiple insertions of the substrate (TEM grids of 3 mm diameter: SPI, model 3520C-CF) into the flame to accumulate enough material for the analysis. Soot samples were analyzed by Raman spectroscopy following the same procedure adopted in [10] and in other previous investigations [18-20]. The grids covered by soot were directly positioned under the Raman microscope (Horiba XploRA) equipped with a 100× objective (NA0.9, Olympus) without further manipulation. The laser source was a Nd:YAG laser (λ = 532 nm, 12 mW maximum laser power at the sample). Spectra were obtained with a laser beam power of 1%, and an accumulation-exposure time of five cycles of 20 s each. For each soot sample deposited on a TEM grid several spots were randomly selected and averaged to obtain a statistically relevant Raman spectrum. Background due to the substrate was verified to be negligible for the analysis of the soot particles signals.

Soot concentration and temperature measurements were performed at pressures of 3, 6, and 10 bar. The optical measurement setup is based on spectral soot emission (SSE), whose details are given in [4] and references therein. Briefly, line-of-sight measurements of spectral radiation was collected within the wavelength range of 690–945 nm. Flames were mapped pointwise using a radial step size of 0.05 mm in horizontal direction (along the radius of the flame) and 0.5 mm in vertical direction. Emission profiles at a given height in the flame were inverted to obtain radially-resolved emission rates from which radial temperature and soot volume fraction distributions could be inferred when soot optical properties are known. A horizontal spatial resolution of 0.07 mm over the depth of field defined by the burner nozzle exit diameter was estimated from knife-edge scans across a diffuse light source located at the object plane. The vertical spatial resolution was inferred to be approximately 0.29 mm.

Results and Discussion

To track the evolution of soot particles, the ethylene laminar diffusion flames operated at several pressures, i.e., 3, 6 and 10 bar, have been preliminary characterized by SSE measurements. Two-dimensional depictions of the soot volume fraction (SVF) measurements for the flame operated under these three pressures are reported in Fig. 2.

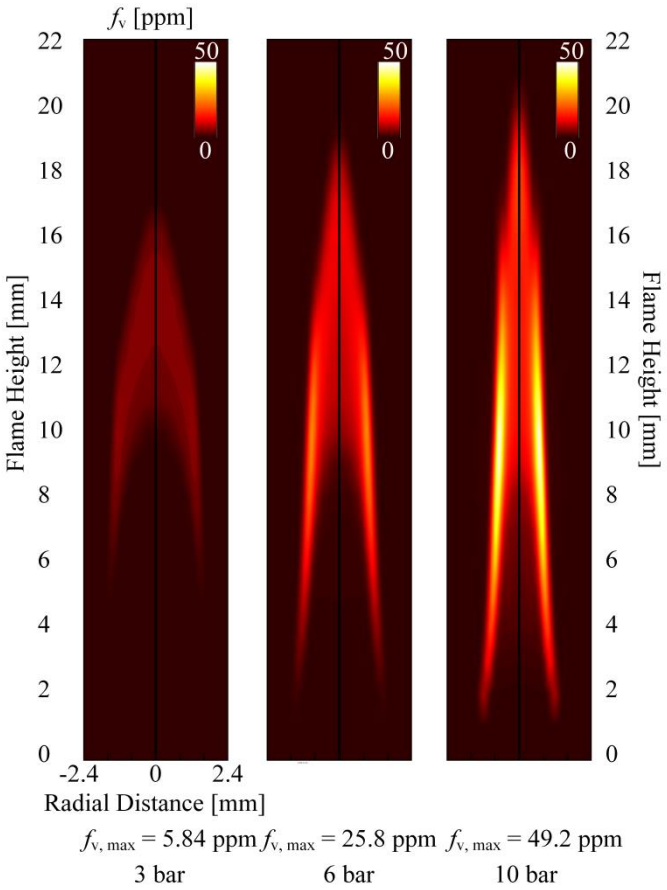

Figure 2. 2D soot volume fraction (SVF) measurements at three different pressures.

SVF significantly increases with increasing pressures as also illustrated by the trend of the maximum soot yield shown in Fig. 3. For all the investigated flames soot reaches its maximum in the annular region at approximatively 10 mm above the burner. Above 10 mm, oxidation causes an overall lowering of the SVF values, leading at the end of the flame in a complete burnout of soot and thus in so called non-smoking flames for pressures below 10 atm. Soot particles, for nanostructure

characterization via Raman spectroscopy analysis, have been therefore collected at 10 mm, for all the flames, corresponding to the maximum SVF location in the investigated flames.

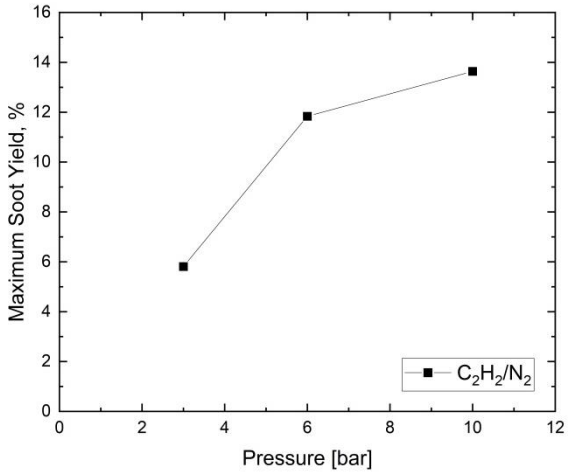

Figure 3. Maximum soot yield vs. pressure.

Raman spectroscopy represents one of the most common and powerful technique for the characterization of carbon materials, and is also commonly used for investigations of the chemical and nanostructure properties of soot particles [18-24]. A typical Raman spectrum of a soot sample is reported in Fig. 4. The spectrum is characterized by the typical two main features of any amorphous carbon, the G band at 1600 cm^{-1} and the D band, at the Raman shift of about 1340 cm^{-1}. Details on the physical origin of these two Raman modes can be found elsewhere [25].

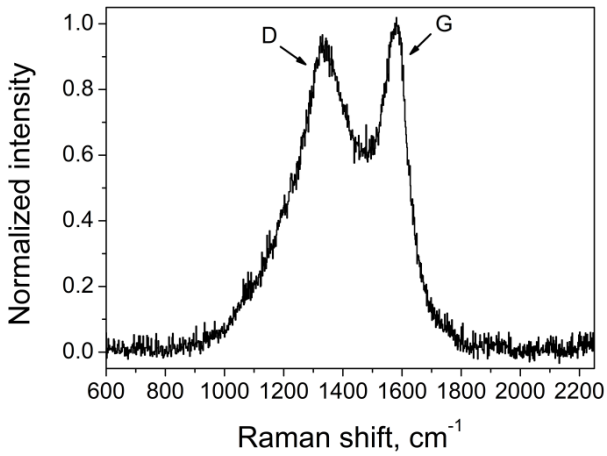

Figure 4. Typical Raman spectrum of collected soot.

Most importantly, it is well recognized that the relative intensity of the D and G peaks, I(D)/I(G), is dependent on the size of graphitic domains, L_a [25]. In case of highly disordered/amorphous carbon materials, i.e., for very small size of the graphite crystallites, as in the case of flame-formed soot particles [18], the following empirical expression has been found to correlate L_a with the relative intensity of the two Raman peaks [25]:

$$L_a^2(\mathrm{nm}^2) = 5.4 \cdot 10^{-2} \cdot E_L^4(\mathrm{eV}^4) \frac{I(\mathrm{D})}{I(\mathrm{G})} \quad (1)$$

where E_L is the energy of the incident photon. The L_a values for soot sampled at different pressures from the same height above the burner rim (10 mm), derived from the corresponding measured Raman spectra, are reported in Fig. 5. Note that the data plotted start from the 2 bar condition because of the insufficient amount of soot that could be collected at 1 bar. The L_a values approximatively range between 1.17 nm to 1.21 nm. Despite the large uncertainties in the L_a values shown in Fig. 5 at all the investigated pressures, the average values indicate an increase of L_a as function of the pressure.

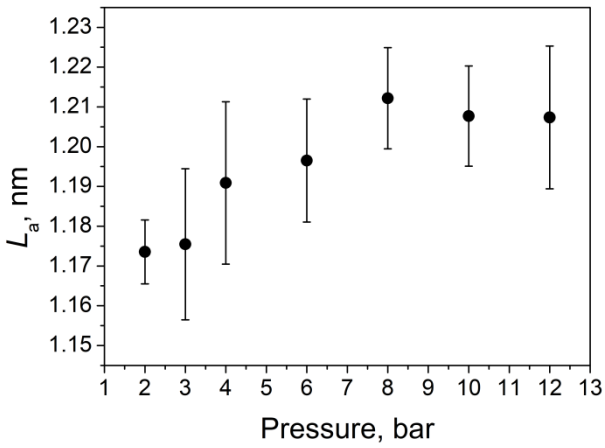

Figure 5. L_a values calculated from the I(D)/I(G) ratios derived from the Raman spectra of soot extracted from flames at different pressures at 10

mm above the burner rim. Error bars correspond to the standard deviations of the experimental data.

These results contrast to those obtained by performing similar analysis on soot particles collected at different pressures from laminar diffusion flames of methane, in which no effect of pressure on soot nanostructure was observed with increasing pressure [10]. In distinction to the previously investigated methane flames, the onset point of soot particle formation in the ethylene flames reported in this work changes with the operating pressure as can be visualized by the vertical shift in the onset of flame luminosity in Fig. 1. and the shift in the soot volume fraction measurements in Fig. 2.

For a more comprehensive analysis of soot inception region and further evolution, detailed radial SFV profiles have been measured, see Fig. 6. Note that measurements were carried out by scanning the entire flame diameter at each height above the burner, and the data reported in Fig. 6 represent the averages of the left and right scans. For the flame operated at 3 bar, soot starts forming in the annular region of the flame and is first detected at 4 mm above the burner by soot emission spectroscopy, and soot concentrations increase by increasing the height above the burner, with a maximum that shifts towards the flame centerline. An increased pressure, from 3 to 6 and 10 bar, results in a lower position of the onset of formation in the flame and a significant overall increase in soot concentration. Indeed, in the flame at 10 bar, soot concentration at 2 mm above the burner is already comparable to the maximum SVF measured in the flame at 3 bar, about 5 ppm.

To summarize, soot particles start forming earlier in the flame as pressure increases. The distance from the onset of formation to the sampling height (where the maximum SVF is reached, 10 mm) changes from about 4.5 mm to roughly 9.5 mm as pressure increases from 1 to 12 bar. This in turn implies that, at a fixed flame height, particle residence time is larger in flames with higher pressure. This observation implies that the particles at the location of maximum volume fraction have underwent different thermal histories in flames with different pressures. This in turn may affect particle properties consistent with the earlier observations reporting that, regardless of the fuel

chemistry, soot inception limit, i.e., the location at which soot starts forming, is the primary factor impacting soot structure and its reactivity towards oxidation [26].

In view of this, it is possible that the observed trend in soot nanostructure in Fig. 5 is due to differences in the thermal aging process as a result of an increase in the particle residence time at 10 mm as a function of pressure. To assess this point further, we also measured the Raman spectra of soot collected at the early stages of formation, i.e., at 2 mm above the burner rim, for the flames operated at 3, 4 and 6 bar. For these conditions, the average size of aromatic domains was in the range of 1.14-1.17 nm, thus lower than that of soot at 10 mm.

It should be noted that sampling with a radial resolution was not possible because of the relatively small flame diameters which are comparable to the TEM sampling grid diameter. Although soot is integrated over the radial flame cross-section, the two samples collected at 2 and 10 mm are well representative of soot particles at the onset and at the maximum volume fraction positions. Indeed, as shown in the soot concentration profiles in Fig. 6, at the soot collection heights of 2 and 10 mm soot inception and maximum volume fraction are mainly located in the annular region of the flames and only a relatively small amount of soot particles is present at inner and outer radial positions. In addition, any further condition, i.e., sampling above 10 mm above the burner, was not investigated in the present work since after the maximum volume fraction is reached soot oxidation reactions become predominant over formation ones.

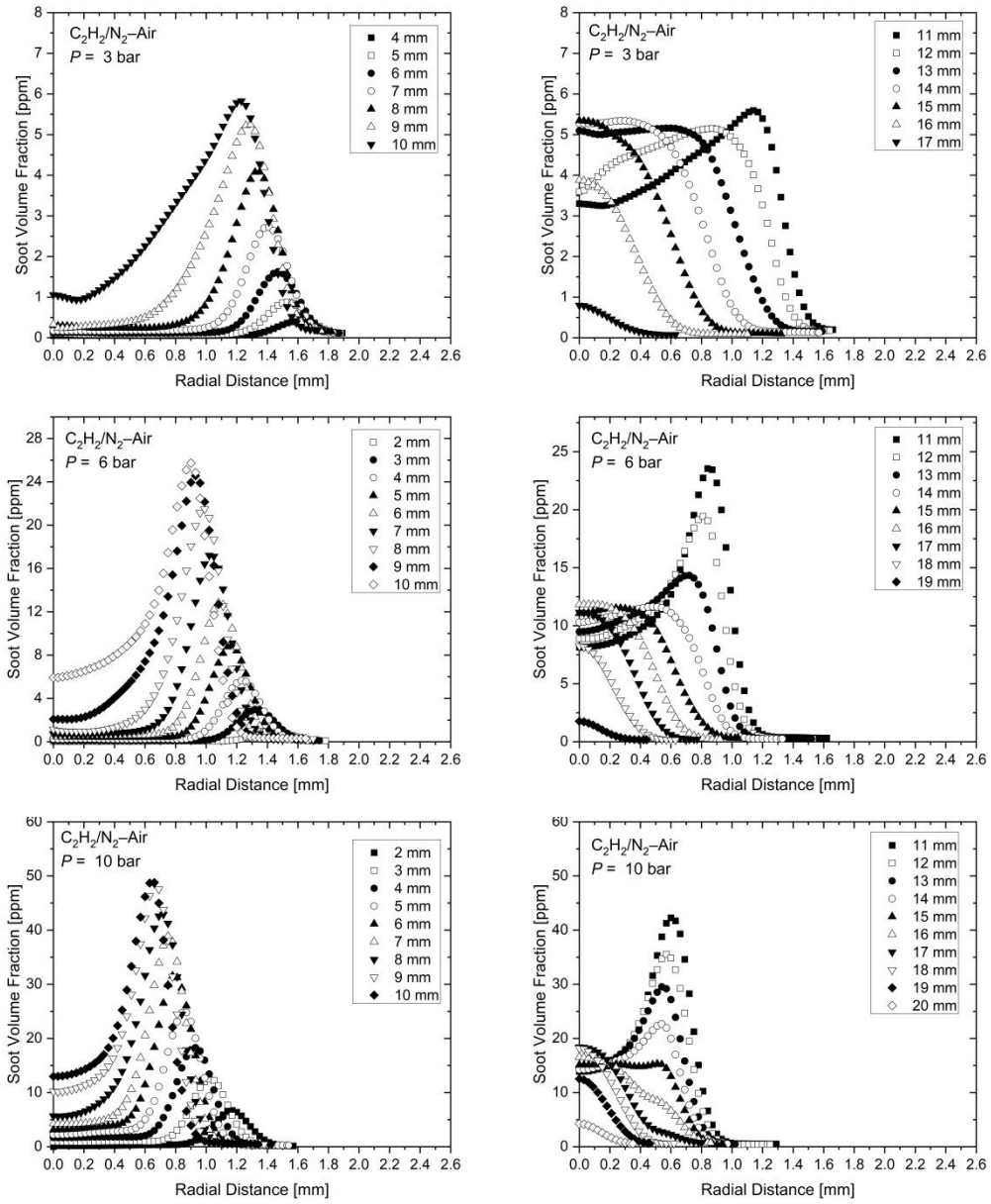

Figure 6. Radially resolved soot volume fraction (SVF) profiles for flames operated at 3, 6 and 10 bar pressure. The plots on the left side refer to the lower half of the flames while the plots on the right side refer to the upper half of the flames (inset numbers refer to the distances from the burner rim).

In order to verify that the observed differences in particle thermal aging are not due to changes in flame temperature, we made detailed flame temperature measurements. As observed from the radial profiles reported in Fig. 7, flame temperatures slightly decrease with increasing pressure due to enhanced radiative heat losses with increasing soot loadings. As a consequence of this, a lower

carbonization rate can be expected since it can be described by a single activation energy Arrhenius model [27, 28]. Since the effect of temperature alone is not consistent with the increase of L_a, we can argue that the change in the particle residence time is the most relevant parameter for soot aging.

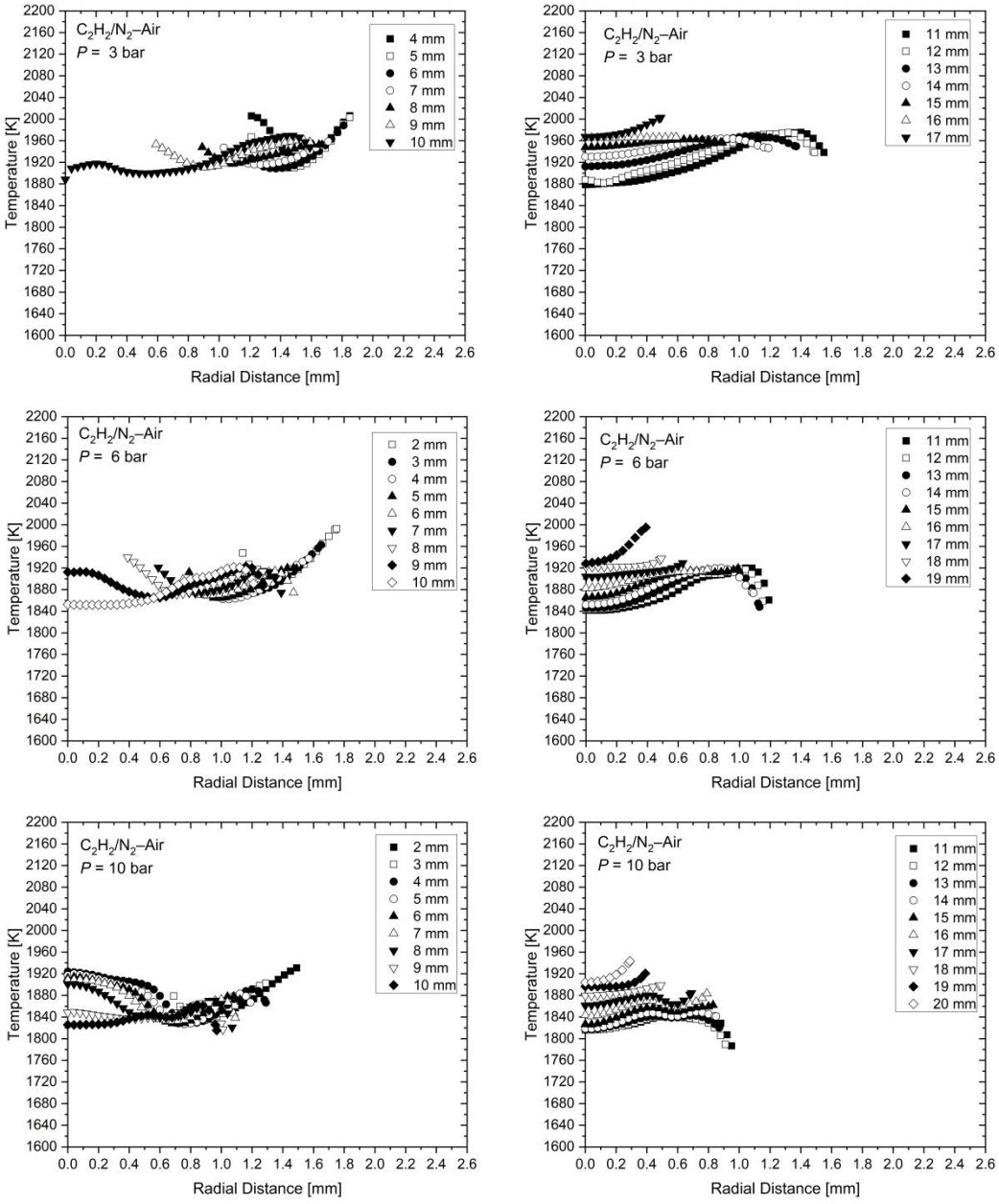

Figure 7. Radially resolved temperature profiles for flames operated at 3, 6 and 10 bar pressure. The plots on the left side refer to the lower half of the flames while the plots on the right side refer to the upper half of the flames (inset numbers refer to the distances from the burner rim).

Consideration of the reaction orders involved in the soot formation process may shed some light on our findings. Soot nucleation via chemical or physical condensation is known to occur through a complex ensemble of second-order reactions [29]. Similarly, the soot particle growth by particle-particle coagulation/coalescence and by surface growth, either by acetylene addition or by physical condensation of other gas-phase molecules, can be all described by bimolecular reactions. These, in turn, result in a strong effect of the pressure on the rates of nucleation, coagulation and surface growth of the soot particles [30]. As a consequence, the pressure increase induces an earlier soot nucleation and faster growth; the former leading to a longer soot particle aging process. The structural rearrangement of carbonaceous materials as well as the growth of the constituent aromatic lamellae in a hot and low-oxygen environment (thermal annealing) may involve isomerization by molecular rearrangement and dehydrogenation [31, 32]. In this regard, a first-order kinetics characteristic of the carbonization/annealing process of soot in flames was found by Dobbins and coauthors [27, 28]. For this process, there would be no apparent dependence on pressure but only on temperature and residence time. In light of this it is clear why the major effect of pressure on the particle properties of soot at the maximum volume fraction point take place through a faster soot inception and longer particle residence time in the flame. It should be noted that in our previous work on high pressure methane flames this effect was not observed, possibly due to the higher values of pressures investigated.

To have a meaningful comparison of the data obtained by Raman spectroscopy at different flame conditions it would be helpful to estimate soot residence times. Flame heights for symmetrical co-flow laminar diffusion flames can be calculated using Roper's correlation [33, 34], which indicates that visible flame heights depend on the mass flow rate of the fuel, independent of pressure. Flames get thinner with increasing pressure, flame cross-sectional diameter being proportional to $P^{-0.5}$ [4]. Then, the average velocity of a gas molecule within the flame envelope and the residence time of the bulk flow, do not change with pressure at a given height. However, as pressure is increased soot is

formed lower within the flame envelope, meaning that at a fixed height the corresponding soot residence time increases with pressure.

The axial velocity, v_z, on flame centreline can be approximated as $v_z(z) = \sqrt{2az}$, where a is an acceleration constant estimated as 41 m/s^2 based on numerical simulations [35, 36]. Then, the residence time of the soot particles on the flame centreline, t, can be predicted from the relationship $t = \sqrt{2z/a}$ and the lower and upper height of the visible soot zone within the centreline. The soot centreline residence time at 10 mm sampling location increases significantly with pressure, from approximatively 5 ms at 1 bar to 18 ms at 12 bar. This suggests that soot samples collected from the same height at different pressures are not always comparable, particularly at the low-pressure range. It should be noted the calculation of the soot residence times in this study from $v_z(z) = \sqrt{2az}$ provides only approximate values for a number of reasons. Foremost, visible flame heights in Fig. 1 show a slight increase within the pressure range suggesting that the flames studied here are not fully developed, i.e., buoyancy dominated. In addition, soot particles follow a more complex trajectory than moving along the centreline [37, 38]. They originate from near the burner rim and drift towards the centreline, making resident time prediction a rather complex task. Finally, it should be emphasized that the above procedure neglects any particles forming or particles being removed by oxidation along their path within the flame between sampling locations. It would be challenging experimentally to account for these; however, detailed numerical simulations might provide a better treatment of the phenomena and it will the subjects of our future investigations.

To assess the effect of residence times on soot maturity, we plotted the L_a values with respect to the centreline soot residence times, as shown in Fig. 8. The observed linear trend supports that the soot maturity, and in particular the L_a value, depends on the soot residence time rather than pressure. Therefore, particle transformation/aging is essentially governed by particle thermal history and only indirectly by pressure through the increase of the residence time of soot in the flame.

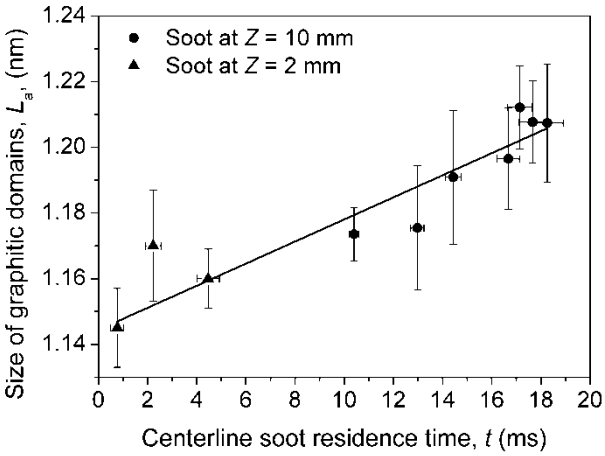

Figure 8. L_a values as a function of predicted centreline soot residence times. Vertical error bars correspond to the standard deviations of the experimental data. Horizontal error bars correspond to the estimated uncertainty in determining the onset of soot formation by SSE measurements. Black line is the result of a linear regression.

It is well known that soot nanostructure strongly affects its propensity to oxidize [5,26], and that soot aging in flames lowers its reactivity towards the oxidation [26,39], therefore our results show that soot formed at high pressures, having a larger residence time in the hot region of the flame where thermal restructuring occurs, is more resistant to oxidation than soot formed at atmospheric conditions.

Conclusions

In this study, we investigated nanostructure of soot particles collected in a set of ethylene laminar diffusion flames at different pressures from 1 to 10atm. Soot volume fraction and temperature measurements by spectral soot emission diagnostic have been performed for flames operated under different pressures. The flame conditions corresponding to soot inception and maximum volume fraction were selected and the corresponding soot particle nanostructure analyzed by Raman spectroscopy.

The results indicate an overall more graphitic structure (a larger size of the aromatic domains) of the fully developed soot particles as pressure increases. Such result is particularly important because of the effect of soot nanostructure on soot oxidative reactivity suggesting that an increase of the pressure has the effect of producing soot more resistant on oxidation.

A more thorough analysis of the data seems to suggest that the increasing pressure affect soot properties indirectly through an earlier inception of the soot particles and thus the increase of the residence time of the soot particles in the flame. Overall, the most effective parameter in determining changes in the soot maturation/graphitization process at higher pressure is nucleation rate.

Acknowledgments

This work was financially supported by Natural Sciences and Engineering Research Council of Canada (RGPIN-2017-06063) and by the “Accordo di Programma CNR-MSE Ricerca di Sistema Elettrico” under the project “MIcro co/tri generazione di Bioenergia Efficiente e Stabile (Mi-Best)”.

References

[1] J.S. Lighty, J.M. Veranth, A.F. Sarofim, Combustion Aerosols: Factors Governing Their Size and Composition and Implications to Human Health, *J. Air & Waste Manage. Assoc.* 50 (2000) 1565-1618.

[2] G. De Falco, C. Colarusso, M. Terlizzi, A. Popolo, M. Pecoraro, M. Commodo, P. Minutolo, M. Sirignano, A. D'Anna, R.P. Aquino, A. Pinto, A. Molino, R. Sorrentino, Chronic obstructive pulmonary disease-derived circulating cells release IL-18 and IL-33 under ultrafine particulate matter exposure in a caspase-1/8-independent manner, *Front. Immunol.* 8 (2017) 1415.

[3] T.C. Bond, S.J. Doherty, D.W. Fahey, P.M. Forster, T. Berntsen, B.J. DeAngelo, et al. Bounding the role of black carbon in the climate system: a scientific assessment. *J. Geophys. Res.: Atmos.* 118 (2013) 5380-552.

[4] A.E. Karataş, O.L. Gülder, Soot formation in high pressure laminar diffusion flames, *Prog. Energy Combust. Science* 38 (2012) 818-845.

[5] R.L. Vander Wal, A.J. Tomasek, Soot oxidation: Dependence upon initial nanostructure. *Combust. Flame* 134 (2003) 1-9.

[6] G.A. Kelesidis, S.E. Pratsinis, Soot light absorption and refractive index during agglomeration and surface growth, *Proc. Combust. Inst.* 37 (2019) 1177-1184.

[7] S.A. Steinmetz, T. Fang, W.L. Roberts, Soot particle size measurements in ethylene diffusion flames at elevated pressures, *Combust. Flame* 169 (2016) 85-93.

[8] A.M. Vargas, Ö.L. Gülder, A multi-probe thermophoretic soot sampling system for high-pressure diffusion flames, *Rev. Sci. Instrum.* 87 (2016), 055101.

[9] A.M. Vargas, Ö.L. Gülder, Pressure dependence of primary soot particle size determined using thermophoretic sampling in laminar methane-air diffusion flames, *Proc. Combust. Institute* 36 (2017) 975-984.

[10] M. Commodo, P.H. Joo, G. De Falco, P. Minutolo, A. D'Anna, Ö.L. Gülder, Raman Spectroscopy of Soot Sampled in High-Pressure Diffusion Flames, *Energy Fuels* 31 (2017) 10158−10164.

[11] P.H. Joo, B. Gigone, E.A. Griffin, M. Christensen, Ö.L. Gülder, Soot primary particle size dependence on combustion pressure in laminar ethylene diffusion flames, *Fuel* 220 (2018) 464-470.

[12] B. Gigone, A.E. Karataş, Ö.L. Gülder, Soot aggregate morphology in coflow laminar ethylene diffusion flames at elevated pressures, *Proc. Combust. Inst.* 37 (2019) 841-848.

[13] H.M.F. Amin, A. Bennett, W.L. Roberts, Determining fractal properties of soot aggregates and primary particle size distribution in counterflow flames up to 10 atm, *Proc. Combust. Inst.* 37 (2019) 1161-1168.

[14] A.D. Sediako, A. Bennett, W.L. Roberts, M.J. Thomson, In Situ Imaging Studies of Combustor Pressure Effects on Soot Oxidation, *Energy Fuels* 33 (2019) 1582-1589.

[15] C.R. Shaddix, K.C.Smyth, Laser-induced incandescence measurements of soot production in steady and flickering methane, propane, and ethylene diffusion flames, *Combust. Flame* 107 (1996) 418-452.

[16] C.S. McEnally, Ü.Ö.Köylü, L.D. Pfefferle, D.E.Rosner, Soot volume fraction and temperature measurements in laminar nonpremixed flames using thermocouples, *Combust. Flame* 109 (1997) 701-720.

[17] T.C. Williams, C.R. Shaddix, K.A. Jensen, J.M. Suo-Anttila, Measurement of the dimensionless extinction coefficient of sootwithin laminar diffusion flames, *Int. J. Heat Mass Transf.* 50 (2007) 1616–1630.

[18] P. Minutolo, M. Commodo, A. Santamaria, G. De Falco, A. D'Anna, Characterization of flame-generated 2-D carbon nano-disks, *Carbon* 68 (2014) 138-148.

[19] M. Commodo, G. De Falco, A. Bruno, C. Borriello, P. Minutolo, A. D'Anna, Physicochemical evolution of nascent soot particles in a laminar premixed flame: from nucleation to early growth, *Combust. Flame* 162 (2015) 3854-63.

[20] M. Commodo, G. De Falco, P. Minutolo, A. D'Anna, Structure and size of soot nanoparticles in laminar premixed flames at different equivalence ratios, *Fuel* 216 (2018) 456-462.

[21] H.J. Seong, A.L. Boehman, Evaluation of Raman Parameters Using Visible Raman Microscopy for Soot Oxidative Reactivity, *Energy Fuels* 27 (2013) 1613-1624.

[22] K.C. Le, C. Lefumeux, P.-E. Bengtsson, T. Pino, Direct observation of aliphatic structures in soot particles produced in low-pressure premixed ethylene flames via online Raman spectroscopy, *Proc. Combust. Inst.* 37 (2019) 869-876.

[23] F. Schulz, M. Commodo, K. Kaiser, G. De Falco, P. Minutolo, G. Meyer, A. D'Anna, and L. Gross. Insights into incipient soot formation by atomic force microscopy. *Proc. Combust. Inst.* 37 (2019) 885-892.

[24] J. Bonpua, Y. Yagües, A. Aleshin, S. Dasappa, J. Camacho, Flame temperature effect on sp^2 bonds on nascent carbon nanoparticles formed in premixed flames ($T_{f,\,max}$ > 2100 K): A Raman spectroscopy and particle mobility sizing study, *Proc. Combust. Inst.* 37 (2019) 943-951.

[25] A.C. Ferrari, J. Robertson, Raman spectroscopy of amorphous, nanostructured, diamond-like carbon, and nanodiamond. *Phil. Trans. R. Soc. Lond. A* 362 (2004) 2477–2512.

[26] H.J. Seong, A.L. Boehman, Studies of soot oxidative reactivity using a diffusion flame burner, *Combust. Flame* 159 (2012) 1864-1875.

[27] R.A. Dobbins, G.J. Govatzidakis, W. Lu, A.F. Schwartzman, R.A. Fletcher, Carbonization rate of soot precursor particles, *Combust. Sci. Tech.* 121 (1996) 103-121.

[28] R.A. Dobbins, Soot Inception Temperature and the Carbonization Rate of Precursor Particles, *Combust. Flame* 130 (2002) 204-214.

[29] H. Wang, Formation of nascent soot and other condensed-phase materials in flames. *Proc. Combust. Inst.* 33 (2011) 41-67.

[30] A. Kazakov, H. Wang, M. Frenklach, Detailed modeling of soot formation in laminar premixed ethylene flames at a pressure of 10 bar, *Combust. Flame* 100 (1995) 111-120.

[31] I.C. Lewis, Chemistry of carbonization, *Carbon* 20 (1982) 519-529.

[32] A. Violi, Cyclodehydrogenation Reactions to Cyclopentafused Polycyclic Aromatic Hydrocarbons, *J. Phys. Chem. A* 109 (2005) 7781-7787.

[33] F.G. Roper, The prediction of laminar jet diffusion flame sizes: Part I. Theoretical model, *Combust. Flame* 29 (1977) 219–226.

[34] F.G. Roper, C. Smith, A.C. Cunningham, The prediction of laminar jet diffusion flame sizes: Part II. Experimental verification, *Combust. Flame* 29 (1977) 227–234.

[35] M.R.J. Charest, C.P.T. Groth, Ö.L. Gülder, A numerical study on the effects of pressure and gravity in laminar ethylene diffusion flames, *Combust. Flame* 158 (2011) 1933–1945.

[36] M.R.J. Charest, C.P.T. Groth, Ö.L. Gülder, Effects of gravity and pressure on laminar co-flow methane-air diffusion flames at pressures from 1 to 60 atmospheres, *Combust. Flame* 158 (2011) 860–875.

[37] Ö.L. Gülder, Corrigendum to "Dependence of sooting characteristics and temperature field of co-flow laminar pure and nitrogen-diluted ethylene–air diffusion flames on pressure"[Combust. Flame 162 (2015) 1566–1574], *Combust. Flame* 173 (2016) 1.

[38] M.R.J. Charest, Ö.L. Gülder, C.P.T. Groth, Numerical and experimental study of soot formation in laminar diffusion flames burning simulated biogas fuels at elevated pressures, *Combust. Flame* 161 (2014) 2678–2691.

[39] J. Camacho, Y. Tao, H. Wang, Kinetics of nascent soot oxidation by molecular oxygen in a flow reactor, *Proc. Combust. Inst.* 35 (2015) 1887–1894.